Human Pathology (2020) 105, 53–66

ELSEVIER

Human PATHOLOGY

www.elsevier.com/locate/humpath

Original contribution

p53 immunostaining cannot be used to predict *TP53* mutations in gastric cancer: results from a large Central European cohort☆,☆☆

Isabelle Schoop MD [a], Saffiyeh Saboor Maleki MSc [a,b], Hans-Michael Behrens PhD [a], Sandra Krüger BSc [a], Jochen Haag PhD [a], Christoph Röcken MD, PhD [a,*]

[a] *Department of Pathology, Christian-Albrechts-University, D-24105 Kiel, Germany*
[b] *Institute for Cardiovascular Prevention, Ludwig Maximilians University, D-80336 Munich, Germany*

Received 11 April 2020; revised 13 September 2020; accepted 14 September 2020

Available online 22 September 2020

Keywords:
Chromosomal instability;
Epstein-Barr virus;
Gastric cancer;
Microsatellite instability;
p53

Summary Four molecular subgroups of gastric cancer (GC) have been proposed, ie, Epstein-Barr virus (EBV)–positive, microsatellite instable, chromosomal instable (CIN), and genomically stable GC. Based on the complex relationship between chromosomal instability and *TP53* mutational status, we hypothesized that the typical clinicopathological characteristics caused by chromosomal instability are correlated with the p53 expression that is detected by immunohistochemistry. Four hundred sixty-seven whole-tissue sections of patients with therapy-naive GC were stained with anti–p53 antibody. The histoscore and staining pattern were analyzed for each slide. Different algorithms of immunohistochemistry evaluation were formed and correlated with clinicopathological characteristics. The algorithms were validated by assessing the mutational status of *TP53* in 111 cases. Four hundred forty-two GCs were p53 positive, and 25 were negative, including 414 GCs with a homogeneous pattern and 53 GCs with a heterogeneous staining pattern. There was no correlation with overall or tumor-specific survival. In comparison with clinicopathological characteristics, the algorithm *high* versus *low* showed correlations with microsatellite instability, hepatocyte growth factor receptor (MET), and *TP53* mutational status. The algorithm *Q1/Q4* versus *Q2/Q3* appeared to be correlated with the phenotype as per the Laurén classification, microsatellite instability, EBV status, and p53 expression pattern. The algorithm $<90\% = 0$ *and* $<50\% = 3+$ *versus* $\geq 90\% = 0$ *or* $\geq 50\% = 3+$ showed correlations with the EBV status, microsatellite instability, grading, and p53 expression pattern. The algorithm *homogeneous* versus *heterogeneous* did not correlate with any clinicopathological characteristic. Our results showed that the immunohistochemistry of p53, *TP53* mutational status, and CIN subtype were connected. However, different algorithms for p53 immunohistochemical evaluation cannot be used to predict *TP53* mutations in CIN GCs in individual cases.

☆ Data of this study were presented in part as a 10 minutes oral presentation at the 102. Annual Meeting of the German Society of Pathology in 2018.
☆☆ Disclosures: None.
* Corresponding author. Department of Pathology, Christian-Albrechts-University, Arnold-Heller-Str. 3, Haus U33, D-24105, Kiel, Germany.
E-mail address: christoph.roecken@uksh.de (C. Röcken).

https://doi.org/10.1016/j.humpath.2020.09.006

1. Introduction

Gastric cancer (GC) is the fifth and sixth most common cancer among men and women in Germany, respectively, leading to 1% of all deaths caused by cancer. It is a disease of the elderly, and the median age is 72 years for men and 75 years for women. However, despite a year survival rate of more than 30%, it is associated with a poor prognosis [1]. Several risk factors are known to lead to gastric neoplasia and cancer, including colonization of the stomach's mucosa by *Helicobacter pylori* and a diet rich in salt [2]. The classification and identification of disease subgroups might help realize more specific and effective therapies to ameliorate both patients' life expectancy and quality of life.

More recently, genetic analyses have provided evidence of the complexity of the genetic alterations present in GC [3–5]. Based on a comprehensive molecular analysis, the Cancer Genome Atlas (TCGA) Research Network proposed the following four molecular subgroups of GC: Epstein-Barr virus–positive (EBV+), microsatellite instable (MSI), chromosomal instable (CIN), and genomically stable (GS) GC. Although EBV+ and MSI GCs can be recognized easily by Epstein–Barr virus-encoded small RNA (EBER) in situ hybridization and microsatellite instability analysis, respectively, recognition of CIN and GS GCs is less straightforward. TCGA distinguished these two groups by the presence or absence of extensive somatic copy number alterations (SCNAs) [3].

Recognition of CIN GCs may be highly important. Chromosomal instability is a driver of intratumoral heterogeneity, which favors the microenvironmental selection and evolution of cancer cell populations, resulting in cancer resistance [6]. However, there is no validated simple diagnostic method for the identification of chromosomal instability besides SCNA analysis or defined molecular markers. TCGA found *TP53* mutations and the loss of the protein's pathway to be one of the key characteristics of CIN GC; 71% of the CIN tumors harbored a *TP53* mutation [3]. Therefore, it is assumed that the detection of *TP53* mutations might be an accurate method to diagnose chromosomal instability in GC. In this context, the immunohistochemistry (IHC) of protein p53 should be discussed as a useful diagnostic tool because some groups have tried to classify this type of cancer based on p53 protein status [7,8,5].

Based on the complex relationship between chromosomal instability and *TP53* mutational status, as well as the detection of p53 *via* IHC, we hypothesized that the typical clinicopathological characteristics caused by chromosomal instability are correlated with the p53 expression that is detected by IHC. A homozygous *TP53* mutation can either lead to the loss of p53 expression or an accumulation of a dysfunctional protein, both of which lead to either a nonstained or a strongly stained p53 immunophenotype in GC nuclei [9,10]. As per other studies, *TP53* mutations can lead to distinct p53 expression types in IHC [11], and an optimized p53 immunohistochemical analysis can be used as a reliable method to detect *TP53* mutations, for example, in ovarian carcinoma [12]. We therefore aimed to find an algorithm for immunohistochemical evaluation to characterize this *TP53 mutation–related p53 expression–type* in GC without genetic analysis [9–12]. To achieve this goal, we assessed p53 expression in a cohort of 467 therapy-naive GCs. Because *TP53* aberration appears to be highly correlated with chromosomal instability, we assumed that typical clinicopathological characteristics, and hence CIN itself, can be represented by the *TP53* mutational status. To verify our results, the mutational status of the gene *TP53* was assessed by Sanger sequencing in a validation cohort of 34 samples of chromosomal instability–enriched (CINe) GCs and 69 samples of *GS* GCs. Because chromosomal instability is connected with intratumoral heterogeneity [6], we paid special attention to an intratumoral heterogeneity of p53 protein expression. Therefore, we reexamined *TP53* in 13 cases with a heterogeneous p53 expression pattern *via* Sanger sequencing.

2. Materials and methods

2.1. Ethics statement

Our project was granted ethical clearance by the local ethics committee of the University Hospital in Kiel, Germany, in agreement with the Helsinki Declaration (D 453/10).

2.2. Patients and tumor samples

We retrospectively examined all patients who had undergone either total or partial gastrectomy for adenocarcinoma of the stomach or gastroesophageal junction between 1997 and 2009. Specimens were obtained from the archive of the Department of Pathology, University Hospital, Kiel. The following patient characteristics were retrieved from the electronic database: age, gender, tumor location, tumor size, depth of the tumor's invasion, number of lymph nodes resected and number of lymph nodes with metastases, distant metastases, stage of disease, invasion into lymphatic vessels, invasion into veins, grading, and residual tumor status. All four subtypes as per TCGA classification were presented [3]. Patients were included if a primary adenocarcinoma of the stomach or gastroesophageal junction was histologically confirmed. They were excluded if histology identified a tumor type other than adenocarcinoma or if patients had undergone perioperative chemotherapy or radiotherapy. This study is also based on the assumption that adenocarcinomas of the gastroesophageal junction and stomach are very similar, basically because many recent studies, most prominently TCGA analyses, have revealed significant genetic overlap of esophageal junctional and gastric adenocarcinomas [3,13].

The date of the patient's death was obtained from the Epidemiological Cancer Registry of the state of Schleswig-

Holstein, Germany. Follow-up data of patients who were still alive were retrieved from hospital records and general practitioners. Our study cohort included formalin-fixed and paraffin-embedded (FFPE) tissue specimens from 467 patients. All patient-related data were pseudonymized after inclusion in the study.

2.3. Assessment of further clinicopathological characteristics

The pathological Tumor-Node-Metastasis (pTNM) stage of all study patients was determined as per the 8th edition of the Union for International Cancer Control guidelines [14]. All tumors were classified as per the Laurén classification [15]. Infection with *H. pylori* was evaluated histologically, using modified Giemsa staining and polymerase chain reaction (PCR). *H. pylori*−specific DNA was detected using a PCR-based assay targeting the 16 S rRNA gene of *H. pylori,* as described previously [16]. EBV-encoded RNA was detected using the EBER probe (Novocastar, Leica Microsystems GmbH, Wetzlar, Germany) and BondMax detection system according to the manufacturer's instructions (Leica Microsystems GmbH), Wetzlar, Germany [17]. Microsatellite instability status was assessed by IHC using antibodies directed against MLH1, PMS2, MSH2, and MSH6. For each case with reduced or absent nuclear staining, subsequent molecular comparison of the allelic profiles of the mononucleotide repeat markers BAT-25, BAT-26, NR-21, NR-24, and NR-27 in the tumor and corresponding normal tissue was carried out [18]. Furthermore, assessment of human epidermal growth factor receptor 2 (HER2) and MET status was performed, as described previously [19,20].

2.4. Immunohistochemistry

Immunohistochemical staining was performed using monoclonal antibodies directed against p53 (clone DO-7; dilution 1:100, Novocastra, Leica Microsystems GmbH, Wetzlar, Germany), using the Bond Max Autostainer (Leica Microsystems GmbH, Wetzlar, Germany). For antigen retrieval, the ER1 antigen retrieval solution was used (20 min, pH 6.0; Leica Microsystems GmbH, Wetzlar, Germany). Peroxidase blocking was carried out using the Bond Polymer Refine Detection Kit DC9800 (Leica Microsystems GmbH, Wetzlar, Germany). Counterstaining was performed with hematoxylin. Immunostaining was evaluated using a Leica microscope (Leica DM 1000; Leica Microsystems, Wetzlar, Germany).

2.5. Immunostaining assessment

Each tumor was assessed using a semiquantitative approach combining intensities of immunostaining and percentages of positive cells of the tumor. The immunostaining intensity of tumor cells showed no (0), weak (1+), moderate (2+), or strong (3+) staining (Fig. 1). The percentage of positive tumor cells showing the defined staining intensities (0, 1+, 2+, 3+) was increased with respect to all tumor cells visible on each tissue specimen, and it always added up to a total of 100% tumor cells.

The HScore was calculated as per the following formula: HScore = [0 × percentage of immunonegative tumor cells]+[1 × percentage of weakly stained tumor cells]+[2 × percentage of moderately stained tumor cells]+[3 × percentage of strongly stained tumor cells], resulting in a possible HScore between 0 and 300. Tumor cells without detectable staining were scored as 0. The maximum possible HScore was 300, if all cells of a given tumor sample showed strong staining: [0 × 0%]+[1 × 0%]+[2 × 0%]+[3 × 100%] = 300.

Because we did not know a priori that the *cutoff* value of p53 expression might be biologically relevant, we applied a stepwise explorative approach (Fig. 2). First, we split the cohort at the median of the HScore, into *low* (HScore <92) and *high* (HScore ≥92) groups, with the *high* group approximating cases with mutated *TP53* (Fig. 2A). Second, we divided the cohort into four quartiles. The outer (Q1: HScore ≤15 and Q4: HScore ≥189) and inner quartiles (Q2: HScore = 16−91 and Q3: HScore = 92−188) were joined to form two new groups: *Q1/Q4* and *Q2/Q3*. Here, the *Q1/Q4* group was assumed to indicate cases with mutated *TP53* (Fig. 2A). Third, we aimed to identify the *TP53* mutation−related p53 expression type by using the raw percentages of the intensities for each tissue specimen. In different permutations of this approach, different percentages of cancer cells showing no (0) or strong (3+) staining were used to group the cohort. For example, specimens showing more than 90% nonstained tumor cells (≥90% = 0) or more than 50% strongly stained tumor cells (>50% = 3+) were grouped as *≥90% = 0 or ≥50% = 3+*", presumably indicating *TP53*-mutated GCs. In this example, the algorithm was *<90% = 0 and <50% = 3+* versus *≥90% = 0 or ≥50% = 3+* (Fig. 2B).

In addition, the pattern of p53 staining was documented. Tumors showing the same staining pattern across the entire tissue specimen were categorized as *homogeneous*. Specifically, *homogeneous white* and *homogeneous black* indicated uniformly negative or positive GCs, and *homogeneous gray* described carcinomas with positively and negatively stained cells next to each other. Tumors with distinct areas of staining intensities in the same slide were categorized as *heterogeneous* (Fig. 3).

2.6. TP53 gene analysis

The cases of the validation cohort (all being EBV negative and microsatellite stable (MSS)) were selected on the basis of Laurén phenotype and HER2 and MET status

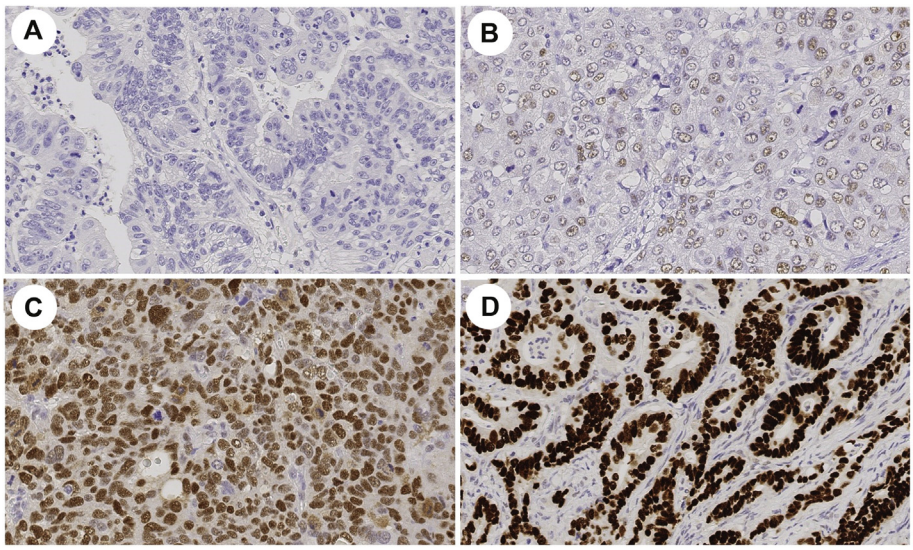

Fig. 1 Reference slides for p53 immunostaining in gastric cancer. Images display the HScore of 0 without staining (A), 1+ with weak staining (B), 2+ with moderate staining (C), and 3+ with strong staining (D). Anti-p53 immunostaining, hematoxylin counterstaining. Original magnifications, ×400.

[3]. HER2/MET-amplified intestinal-type cases were equated with putative CINe GCs, and HER2/MET-non-amplified diffuse-type cases were equated with GS GCs. The *TP53* mutational status was assessed in 111 GCs, containing 34 CINe and 69 *GS* GCs; 13 GCs with a heterogeneous p53 pattern received independent gene analyses in both areas.

2.7. DNA extraction

The tumor DNA was extracted from the FFPE tumor blocks using the AllPrep DNA/RNA FFPE Kit (Qiagen GmbH, Hilden, Germany) or the QIAamp DNA Mini kit (Qiagen GmbH, Hilden, Germany), depending on the availability of the kits.

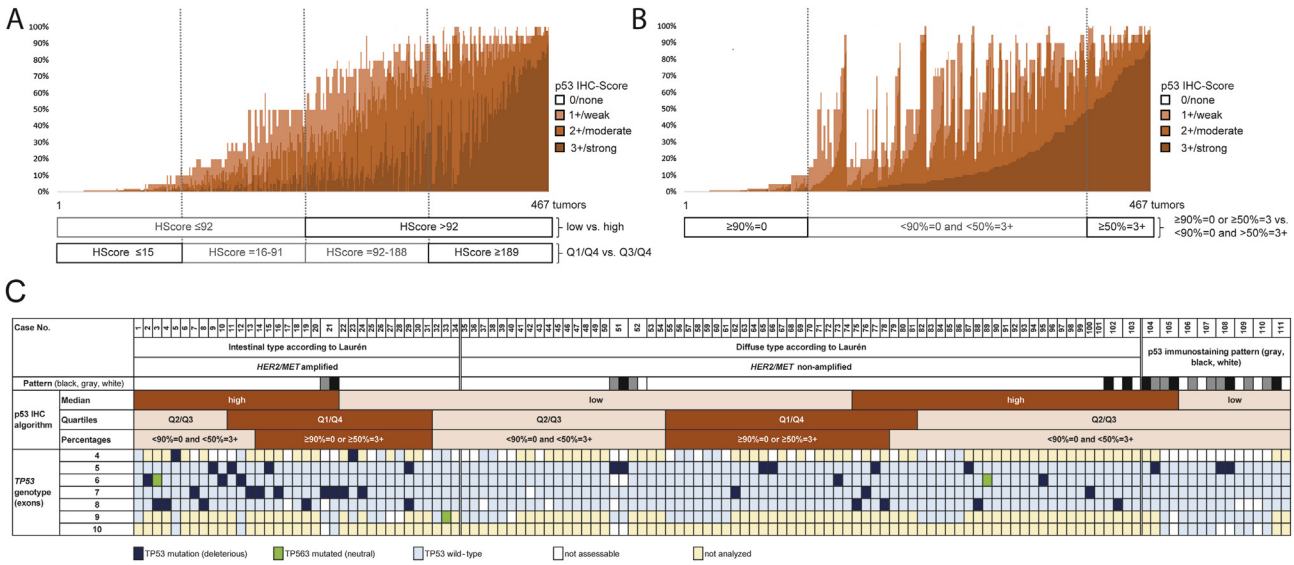

Fig. 2 Evaluation of p53 immunostaining in a cohort of 467 patients with gastric cancer. The colors represent the percentage area of tumor in each case showing no (0), weak (1+), moderate (2+), or strong (3+) p53 immunostaining. The histogram finally illustrates the distribution pattern of the staining patterns of the entire cohort in a single graph. A, The results of p53 immunostaining are sorted as per the HScore; the first algorithm *low* vs. *high* and the second algorithm *Q1/Q4* vs. *Q2/Q3* are supplemented. B, The results of p53 IHC are sorted by percentages; the third evaluation algorithm $<90\% = 0$ *and* $<50\% = 3+$ vs. $\geq 90\% = 0$ *or* $\geq 50\% = 3+$ is supplemented. C, Validation of *TP53* mutational status in 111 cases. HER2/MET-amplified, intestinal-type GCs are considered to be CINe, while HER2/MET-nonamplified and diffuse-type GCs are equated with GS GCs. The case no. 21, 51, 52, and 102−111 are GCs with a heterogeneous staining pattern, and the TP53 mutational status was analyzed in both areas independently. Immunohistochemical evaluation algorithms are added. CINe, chromosomal instability−enriched; GC, gastric cancer; GS, genomically stable; HER2, human epidermal growth factor receptor 2; IHC, immunohistochemistry; MET, hepatocyte growth factor receptor.

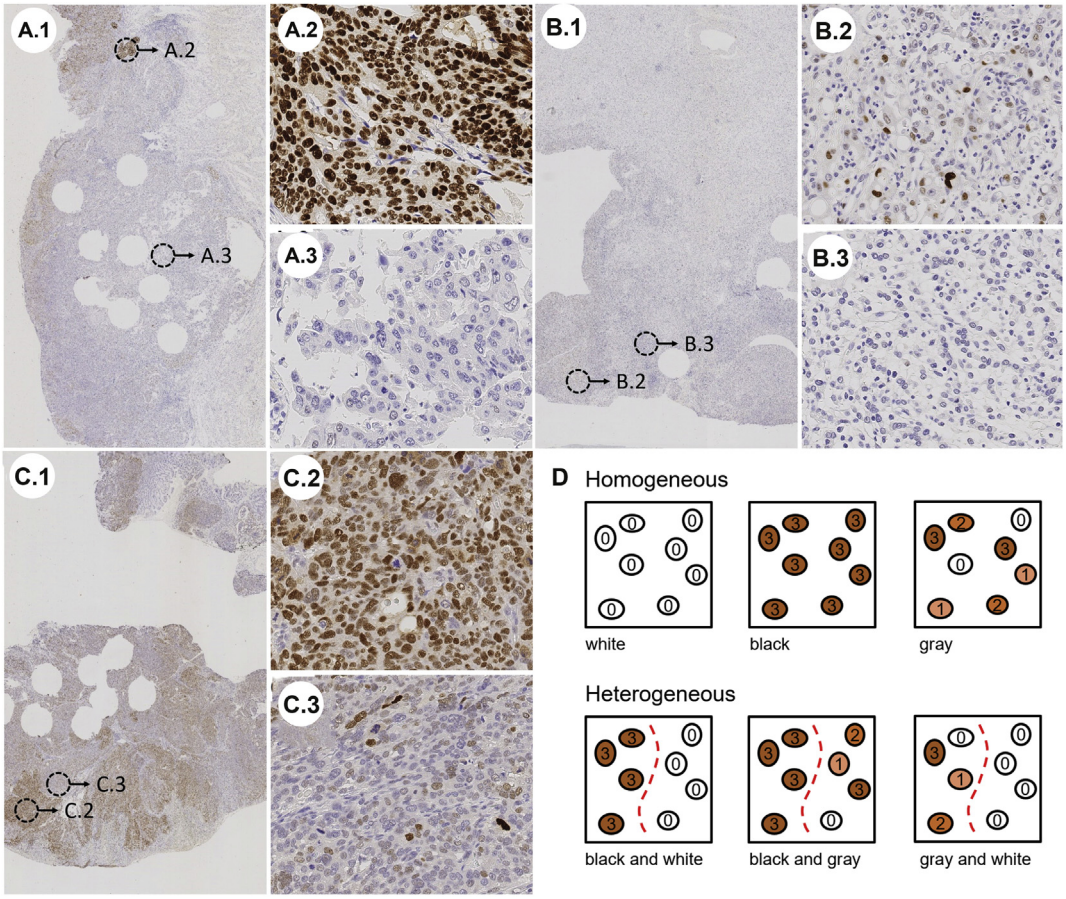

Fig. 3 Heterogeneous cases of p53 immunostaining. A, Heterogeneous black and white: overview (A.1), black (A.2), and white (A.3); B, heterogeneous gray and white: overview (B.1), gray (B.2), and white (B.3); C, heterogeneous black and gray: overview (C.1), black (C.2), and gray (C.3). D, Scheme of the analysis of the immunostaining pattern. *Homogeneous white* and *black* named uniformly negative or positive GCs. *Homogeneous gray* described carcinomas with positively and negatively stained cells next to each other. *Heterogeneous* was chosen for tumors with distinct areas of staining intensities in the same slide. Anti-p53 immunostaining, hematoxylin counterstaining. Original magnifications: ×1 (A.1, B.1, C.1), ×400 (A.2, A.3, B.2, B.3, C.2, C.3). GC, gastric cancer.

(1) Extraction using the AllPrep DNA/RNA FFPE Kit: Each sample (300 mm^2) was cut out of 10- to 20-µm-thick paraffin sections and deparaffinized with 1 ml of xylene. After washing the samples with 1 ml of 96% ethanol and drying them off, 150 µl of buffer PKD and 10 µl of proteinase K were added to each sample. The tubes were incubated at 56 °C for 15 min and subsequently incubated on ice for 3 min. Centrifugation was performed (20,000× g, 15 min), and the pellet was resuspended in 180 µl of buffer ATL and 40 µl of proteinase K. After mixing, the samples were incubated at 56 °C and 90 °C for 1 h and 2 h, respectively. Next, 200 µl of buffer AL and 200 µl of ethanol (96%) were added to each sample. The samples were then transferred to a *QIAamp MinElute spin column* (Qiagen GmbH, Hilden, Germany) and centrifuged at 8000×*g* for 1 min. The columns were washed twice with 700 µl of buffer AW1 and buffer AW2, respectively, and dehydrated using 700 µl of 96% ethanol. Finally, 50 µl of buffer ATE was added to the center of each column, and the DNA was eluted after 1 min of incubation.

(2) Extraction using the QIAamp DNA Mini kit: For each case, up to six tissue sections (5−10 µm) were deparaffinized with xylene and afterward washed with 99% ethanol. After drying off the samples, tumor DNA extraction was performed using disposable scalpels. One hundred eighty microliters of buffer ATL and 20 µl of proteinase K were added to each sample. The tubes were incubated at 56 °C for at least 2 h and afterward at 90 °C for 20 min using the Thermomixer comfort (Eppendorf, Hamburg, Germany). Next, 200 µl of buffer AL was added, and the samples were incubated at 70 °C for 10 min. After adding 200 µl of ethanol (96%) to each sample, it then was transferred to a *QIAamp Mini Spin Column* and centrifuged at 6000× *g* for 1 min. The columns were washed twice with 500 µl of buffer AW1 and buffer AW2, respectively. Finally, 50 µl of buffer AE was added to the center of each column, and the DNA was eluted after 1 min of incubation.

Nucleic acid concentrations were assessed using NanoDrop 2000c (Thermo Scientific, Wilmington, DE, USA).

2.8. PCR of TP53 exons

The *TP53* exons (4−10) were amplified using the PyroMark PCR kit (Qiagen, Germany) using different primers (Supplemental Table 1). The amplification reaction was carried out for 45 cycles at 95°C for 30 s, 55°C for 45 s, and 72°C for 45 s. Samples were run on gels to ensure the quality and length of the amplified regions. The PCR products were purified using the QIAquick® 96 PCR Purification kit (Qiagen, Germany) or NucleoSpin® PCR Clean-up kit (Macherey-Nagel, Düren, Germany).

2.9. TP53 sequencing

Sequencing was carried out using the BigDye® Terminator v1.1 Cycle sequencing kit (Thermo Fisher Scientific Baltics, Vilnius, Lithuania). One microliter of each PCR product (10 ng/µl) was added to a mixture containing 2 µl of BigDye® Terminator v1.1 Ready Reaction Mix, 2 µl of BigDye® Terminator v1.1 sequencing buffer, 14.5 µl of deionized water (RNase/DNase-free), and 0.5 µl of either forward or reverse primers (3.2 pmol). The sequencing reaction was then performed in 27 cycles at 96°C for 20 s, 50°C for 10 s, and 60°C for 4 min. The sequencing reaction products were purified using a NucleoSEQ® clean-up kit (Macherey-Nagel, Germany). Purified DNA sequences were subjected to capillary electrophoresis on a 3500 Series Genetic Analyzer (Applied Biosystems, Darmstadt, Germany). The electropherograms were observed using Finch TV version 4 software (Digital World Biology, Seattle, WA, USA), and mutations were detected by comparing exon sequences to the reference coding sequence (CCDS 11118.1) (Serial Cloner 2.1). The type of mutation was inspected with the aid of Cosmic and IARC TP53 data sets.

2.10. Statistical analysis

SPSS version 25.0.0.2 (IBM Corp., Armonk, NY) was used for statistical analyses. Correlation between non-ordinal variables was ascertained using Fisher's exact test, whereas that between ordinal variables was ascertained using Kendall's tau test. We assumed a significance level of 0.05. To compensate for the false discovery rate (FDR) within the correlations, we applied the Simes (Benjamini-Hochberg) procedure (FDR correction) [21]. All *P*-values are uncorrected. The *P*-values that remained significant after FDR correction have been indicated in Table 1. Median survival with 95% confidence intervals was determined using the Kaplan-Meier method. Differences between median survival rates were tested using the log-rank test.

3. Results

In total, 467 patients fulfilled all study criteria. The clinicopathological characteristics of the patients have been summarized in Table 1. Among them, 19 cases were EBV negative, whereas the EBV status was unknown in 14 cases. Furthermore, 34 cases appeared to be MSI, but the microsatellite instability status was missing in 16 cases. As per Laurén classification [15], 149 GCs showed a diffuse phenotype, whereas 318 cases were classified as intestinal, mixed, or unclassifiable. Considering overlaps among these groups, after EBV+ GC, MSI GC, and diffuse-type GCs as per Laurén classification [15] were subtracted, 254 EBV-negative, MSS, and non-diffuse cases were classified as CINe (Fig. 4).

Overall survival (OS) and tumor-specific survival (TSS) data were available for 455 (97.4%) and 426 (91.2%) of the 467 cases, respectively. The mean follow-up period was 12.8 months (range, 0 to 142.7 months). The median OS was 14.9 months, and the median TSS was 16.6 months.

3.1. Immunohistochemistry

p53 expression was studied using whole-tissue sections. Nuclear immunostaining was found in tumor cells, non-neoplastic mucosa cells, stromal cells, endothelial cells, and lymphocytes. Among the 467 cases, 442 (94.6%) showed p53 immunostaining, whereas 25 (5.4%) cases were completely p53 immunonegative. In 117 (25.1%) cases, at least 90% of tumor cells were homogeneously p53 negative. The percentage of stained tumor cells ranged from 0% to 100% (median = 50.0%). Staining intensities ranged from 0 (no staining) to 3 (strong staining). The HScore calculated by the percentages for each intensity in the tumor ranged from 0 to 285, with a median of 92 (Supplemental Fig. 1). A total of 414 (88.7%) cases harbored a homogeneous staining pattern, and 53 (11.3%) had a heterogeneous staining pattern.

3.2. Correlation with clinicopathological characteristics

The results have been summarized in Table 1. None of the approaches for evaluating the p53 immunostaining pattern correlated with the OS or TSS (Table 1 and Fig. 5).

3.2.1. First algorithm: p53 HScore divided at the median (*low* versus *high*)

When the HScore was dichotomized at the median into *high* and *low*, p53 status correlated significantly with MSI ($P = 0.001$) and MET status ($P = 0.005$) (Table 1). Regarding the 254 EBV-negative, MSS, and non-diffuse GCs, the *low* group harbored 109 (42.9%) cases, whereas the *high* group harbored 145 (57.1%) cases (Fig. 4).

3.2.2. Second algorithm: p53 HScore divided into quartiles (*Q2/Q3* versus *Q1/Q4*)

When the HScore status was categorized into *Q1/Q4* and *Q2/Q3*, the p53 status correlated with the intestinal phenotype as per Laurén classification ($P = 0.041$) and

Table 1 Evaluation algorithms for p53 immunostaining and correlation with clinicopathological patient characteristics.

Clinicopathological characteristic		Valid/missing [n]		First algorithm				Second algorithm				Third algorithm				Pattern of p53 immunostaining			
				Median				Quartiles				Percentages							
				Low		High		Q2/Q3		Q1/Q4		<90% = 0 and <50% = 3		≥90% = 0 or ≥50% = 0		Homogeneous		Heterogeneous	
		n	(%)	n	(%)	n	(%)		(%)	n	(%)	n	(%)	n	(%)	n	(%)	n	(%)
Age (years)	p[a]	467/0					p = 0.405				p = 0.579				p = 0.345				p = 0.468
<68		235	(50.3)	122	(51.9)	113	(48.1)	120	(51.1)	115	(48.9)	135	(57.4)	100	(42.6)	211	(89.8)	24	(10.2)
≥68		232	(49.7)	111	(47.8)	121	(52.2)	112	(48.3)	120	(51.7)	144	(62.1)	88	(37.9)	203	(87.5)	29	(12.5)
Gender	p[a]	467/0					p > 0.999				p > 0.999				p = 0.628				p = 0.882
Female		181	(38.8)	90	(49.7)	91	(50.3)	90	(49.7)	91	(50.3)	111	(61.3)	70	(38.7)	160	(88.4)	21	(11.6)
Male		286	(61.2)	143	(50.0)	143	(50.0)	142	(49.7)	144	(50.3)	168	(58.7)	118	(41.3)	254	(88.8)	32	(11.2)
Localization	p[a]	466/1					p = 0.072				p = 0.368				p > 0.999				p = 0.529
Proximal		145	(31.1)	63	(43.4)	82	(56.6)	67	(46.2)	78	(53.8)	87	(60.0)	58	(40.0)	131	(90.3)	14	(9.7)
Distal		321	(68.9)	169	(52.6)	152	(47.4)	164	(51.1)	157	(48.9)	191	(59.5)	130	(40.5)	282	(87.9)	39	(12.1)
Laurén phenotype	p[a]	467/0					p = 0.338				p = 0.041				p = 0.893				p = 0.222
Intestinal		238	(51.0)	115	(48.3)	123	(51.7)	103	(43.3)	135	(56.7)	138	(58.0)	100	(42.0)	208	(87.4)	30	(12.6)
Diffuse		149	(31.9)	82	(55.0)	67	(45.0)	85	(57.0)	64	(43.0)	92	(61.7)	57	(38.3)	138	(92.6)	11	(7.4)
Mixed		31	(6.6)	12	(38.7)	19	(61.3)	18	(58.1)	13	(41.9)	19	(61.3)	12	(38.7)	26	(83.9)	5	(16.1)
Unclassifiable		49	(10.5)	24	(49.0)	25	(51.0)	26	(53.1)	23	(46.9)	30	(61.2)	19	(38.8)	42	(85.7)	7	(14.3)
pT category	p[a]	467/0					p = 0.529				p = 0.383				p = 0.731				p = 0.918
T1a/T1b		60	(12.8)	32	(53.3)	28	(46.7)	19	(31.7)	41	(68.3)	27	(45.0)	33	(55.0)	56	(93.3)	4	(6.7)
T2		53	(11.3)	28	(52.8)	25	(47.2)	30	(56.6)	23	(43.4)	31	(58.5)	22	(41.5)	47	(88.7)	6	(11.3)
T3		184	(39.4)	90	(48.9)	94	(51.1)	100	(54.3)	84	(45.7)	126	(68.5)	58	(31.5)	157	(85.3)	27	(14.7)
T4a/T4b		170	(36.4)	83	(48.8)	87	(51.2)	83	(48.8)	87	(51.2)	95	(55.9)	75	(44.1)	154	(90.6)	16	(9.4)
pN category	p[a]	466/1					p = 0.691				p = 0.529				p = 0.444				p = 0.705
N0		136	(29.2)	75	(55.1)	61	(44.9)	73	(53.7)	63	(46.3)	79	(58.1)	57	(41.9)	122	(89.7)	14	(10.3)
N1		63	(13.5)	27	(42.9)	36	(57.1)	25	(39.7)	38	(60.3)	35	(55.6)	28	(44.4)	57	(90.5)	6	(9.5)
N2		82	(17.6)	35	(42.7)	47	(57.3)	44	(53.7)	38	(46.3)	50	(61.0)	32	(39.0)	70	(85.4)	12	(14.6)
N3		185	(39.7)	95	(51.4)	90	(48.6)	89	(48.1)	96	(51.9)	114	(61.6)	71	(38.4)	164	(88.6)	21	(11.4)
Lymph node ratio	p[a]	466/1					p = 0.578				p = 0.517				p > 0.999				p > 0.999
<0.189		228	(48.9)	117	(51.3)	111	(48.7)	117	(51.3)	111	(48.7)	136	(59.6)	92	(40.4)	202	(88.6)	26	(11.4)
≥0.189		238	(51.1)	115	(48.3)	123	(51.7)	114	(47.9)	124	(52.1)	142	(59.7)	96	(40.3)	211	(88.7)	27	(11.3)
pM category	p[a]	467/0					p = 0.408				p = 0.344				p = 0.228				p = 0.265
M0		379	(81.2)	193	(50.9)	186	(49.1)	184	(48.5)	195	(51.5)	221	(58.3)	158	(41.7)	339	(89.4)	40	(10.6)
M1		88	(18.8)	40	(45.5)	48	(54.5)	48	(54.5)	40	(45.5)	58	(65.9)	30	(34.1)	75	(85.2)	13	(14.8)
UICC stage	p[b]	466/1					p = 0.404				p = 0.175				p = 0.072				p = 0.170
IA/IB		83	(17.8)	45	(54.2)	38	(45.8)	35	(42.2)	48	(57.8)	41	(49.4)	42	(50.6)	78	(94.0)	5	(6.0)
IIA/IIB		98	(21.0)	47	(48.0)	51	(52.0)	50	(51.0)	48	(49.0)	61	(62.2)	37	(37.8)	85	(86.7)	13	(13.3)
IIIA/IIIB/IIIC		197	(42.3)	100	(50.8)	97	(49.2)	98	(49.7)	99	(50.3)	118	(59.9)	79	(40.1)	175	(88.8)	22	(11.2)
IV		88	(188.9)	40	(45.5)	48	(54.5)	48	(54.5)	40	(45.5)	58	(65.9)	30	(34.1)	75	(85.2)	13	(14.8)
pL category	p[a]	449/18					p = 0.187				p = 0.637				p = 0.701				p = 0.465
L0		220	(49.0)	116	(52.7)	104	(47.3)	112	(50.9)	108	(49.1)	129	(58.6)	91	(41.4)	192	(87.3)	28	(12.7)
L1		229	(51.0)	106	(46.3)	123	(53.7)	111	(48.5)	118	(51.5)	139	(60.7)	90	(39.3)	205	(89.5)	24	(10.5)
pV category	p[a]	448/19					p = 0.763				p = 0.546		p = 0.645						p = 0.815
V0		399	(89.1)	200	(50.1)	199	(49.9)	200	(50.1)	199	(49.9)	235	(58.9)	164	(41.1)	353	(88.5)	46	(11.5)
V1		49	(10.9)	23	(46.9)	26	(53.1)	22	(44.9)	27	(55.1)	31	(63.3)	18	(36.7)	43	(87.8)	6	(12.2)
Grading	p[a]	467/0					p = 0.128				p = 0.064				p = 0.035				p = 0.392
G1/G2		110	(23.6)	62	(56.4)	48	(43.6)	46	(41.8)	64	(58.2)	56	(50.9)	54	(49.1)	95	(86.4)	15	(13.6)
G3/G4		357	(76.4)	171	(47.9)	186	(52.1)	186	(52.1)	171	(47.9)	223	(62.5)	134	(37.5)	319	(89.4)	38	(10.6)
R status	p[a]	464/3					p = 0.674				p = 0.889				p > 0.999				p = 0.827
R0		406	(87.5)	205	(50.5)	201	(49.5)	202	(49.8)	204	(50.2)	242	(59.6)	164	(40.4)	360	(88.7)	46	(11.3)
R1		58	(12.5)	27	(46.6)	31	(53.4)	28	(48.3)	30	(51.7)	35	(60.3)	23	(39.7)	51	(87.9)	7	(12.1)
H. pylori status	p[a]	396/71					p = 0.579				p = 0.890				p = 0.322				p = 0.108
Negative		335	(84.6)	174	(51.9)	161	(48.1)	165	(49.3)	170	(50.7)	194	(57.9)	141	(42.1)	304	(90.7)	31	(9.3)
Positive		61	(15.4)	29	(47.5)	32	(52.5)	31	(50.8)	30	(49.2)	40	(65.6)	21	(34.4)	51	(83.6)	10	(16.4)

(continued on next page)

Table 1 (continued)

Clinicopathological characteristic		Valid/missing [n]		First algorithm				Second algorithm				Third algorithm				Pattern of p53 immunostaining			
				Median				Quartiles				Percentages							
				Low		High		Q2/Q3		Q1/Q4		<90% = 0 and <50% = 3		≥90% = 0 or ≥50% = 0		Homogeneous		Heterogeneous	
		n	(%)	n	(%)	n	(%)		(%)	n	(%)	n	(%)	n	(%)	n	(%)	n	(%)
EBV status	p[a]	453/14					p = 0.490				p < 0.001[d]				p = 0.007				p = 0.146
Negative		434	(95.8)	213	(49.1)	221	(50.9)	205	(47.2)	229	(52.8)	252	(58.1)	182	(41.9)	388	(89.4)	46	(10.6)
Positive		19	(4.2)	11	(57.9)	8	(42.1)	17	(89.5)	2	(10.5)	17	(89.5)	2	(10.5)	15	(78.9)	4	(21.1)
MSI status	p[a]	451/16					p = 0.001[d]				p < 0.001[d]				p = 0.017				p = 0.574
MSS		417	(92.5)	197	(47.2)	220	(52.8)	194	(46.5)	223	(53.5)	241	(57.8)	176	(42.2)	370	(88.7)	47	(11.3)
MSI		34	(7.5)	26	(76.5)	8	(23.5)	27	(79.4)	7	(20.6)	27	(79.4)	7	(20.6)	29	(85.3)	5	(14.7)
HER2 status	p[a]	437/30					p = 0.296				p = 0.223				p = 0.109				p = 0.290
Negative		401	(91.8)	198	(49.4)	203	(50.6)	204	(50.9)	197	(49.1)	247	(61.6)	154	(38.4)	356	(88.8)	45	(11.2)
Positive		36	(8.2)	14	(38.9)	22	(61.1)	14	(38.9)	22	(61.1)	17	(47.2)	19	(52.8)	30	(83.3)	6	(16.7)
MET status	p[a]	455/12					p = 0.005				p = 0.278				p = 0.456				p > 0.999
Negative		423	(93.0)	217	(51.3)	206	(48.7)	215	(50.8)	208	(49.2)	256	(60.5)	167	(39.5)	374	(88.4)	49	(11.6)
Positive		32	(7.0)	8	(25.0)	24	(75.0)	13	(40.6)	19	(59.4)	17	(53.1)	15	(46.9)	29	(90.6)	3	(9.4)
TP53 mutational status	p[a]	111/356					p < 0.001[d]				p = 0.101				p = 0.210				p = 0.101
WT or silent mutation		75	(67.6)	49	(65.3)	26	(34.7)	47	(62.7)	28	(37.3)	50	(66.7)	25	(33.3)	66	(88.0)	9	(12.0)
Mutation other than silent mutation		36	(32.4)	10	(27.8)	26	(72.2)	16	(44.4)	20	(55.6)	19	(52.8)	17	(47.2)	27	(75.0)	9	(25.0)
p53 expression pattern	p[a]	467/0					p = 0.243				p < 0.001[d]				p = 0.037				
Homogeneous		414	(88.7)	211	(51.0)	203	(49.0)	192	(46.4)	222	(53.6)	240	(58.0)	174	(42.0)				
Heterogeneous		53	(11.3)	22	(41.5)	31	(58.5)	40	(75.5)	13	(24.5)	39	(73.6)	14	(26.4)				
Overall survival (months)	p[c]						p = 0.089				p = 0.547				p = 0.062				p = 0.612
Total/events/censored		455/352/103		226/163/63		229/189/40		225/178/47		230/174/56		273/223/50		182/129/53		403/309/94		52/43/9	
Median survival		14.9 ± 1.1		16.5 ± 2.1		14.6 ± 1.3		14.6 ± 1.9		15.0 ± 1.4		14.7 ± 1.5		15.0 ± 1.9		14.7 ± 1.1		17.9 ± 3.8	
95% CI		12.7–17.0		12.5–20.6		12.0–17.2		10.8–18.4		12.2–17.7		11.7–17.7		11.2–18.8		12.5–16.9		10.5–25.4	
Tumor-specific survival (months)	p[c]						p = 0.110				p = 0.805				p = 0.171				p = 0.569
Total/events/censored		426/287/139		213/133/80		213/154/59		214/145/69		212/142/70		257/180/77		169/107/62		379/252/127		47/35/12	
Median survival		16.6 ± 1.4		18.1 ± 3.6		15.4 ± 1.7		16.6 ± 2.7		16.6 ± 1.6		16.6 ± 1.6		16.7 ± 2.5		16.5 ± 1.5		18.2 ± 4.1	
95% CI		13.8–19.4		11.0–25.2		12.1–18.7		11.3–22.0		13.4–19.7		13.4–19.8		11.8–21.6		13.5–19.5		10.2–26.2	

Abbreviations: CI, confidence interval; EBV, Epstein-Barr virus; FDR, false discovery rate; HER2, human epidermal growth factor receptor 2; MET, Hepatocyte growth factor receptor; MSI, microsatellite instable; MSS, microsatellite stable; UICC, Union for International Cancer Control; WT, wild-type.

[a] p values were obtained using Fisher's exact test.

[b] p values were obtained using Kendall's tau test.

[c] p values were obtained using the log-rank test.

[d] Significant after FDR correction.

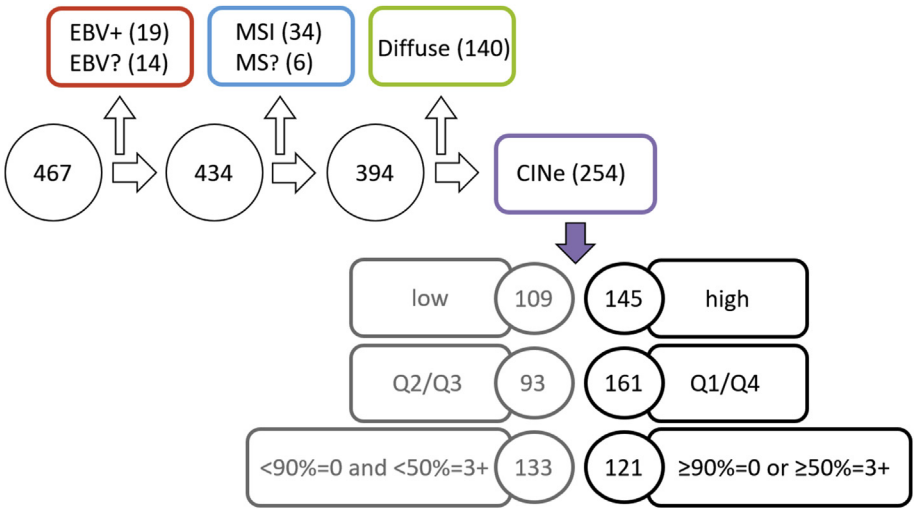

Fig. 4 Sorting out all Epstein-Barr virus−positive (EBV+) and microsatellite instable (MSI) GCs, cases with a diffuse-type histology and unknown EBV (EBV?) or microsatellite status (MS?) considering all overlaps among these groups, 254 EBV-negative, microsatellite stable, and nondiffuse cases were counted. Regarding the different immunostaining evaluation algorithms, the *high* group harbored 145 cases, the *Q1/Q4* group contained 164 cases, and the *≥90% = 0 or ≥50% = 3+* group contained 121 cases. CINe, chromosomal instability−enriched; GC, gastric cancer.

MSS ($P < 0.001$), and EBV status ($P < 0.001$) (Table 1). Regarding the 254 EBV-negative, MSS, and non-diffuse GCs, the *Q2/Q3* group contained 93 (36.6%) cases, whereas the *Q1/Q4* group contained 161 (63.4%) cases (Fig. 4).

3.2.3. Third algorithm: p53 status divided by raw percentages

We also explored in a stepwise procedure the putative cutoff values of p53 immunostaining using raw percentages. Different approaches of algorithms were correlated with the phenotype as per Laurén classification and EBV, microsatellite instability, HER2, and MET status. The categorization into *≥90% = 0 or ≥70% = 3+* vs. remainders showed a correlation with EBV negativity ($P = 0.027$). Categorization into *≥99% = 0 or ≥70% = 3+* ($P = 0.004$) and *≥99% = 0 or ≥80% = 3+* ($P = 0.017$) vs. remainder correlated with MSS. The *≥99% = 0 or ≥50% = 3+* group correlated with EBV negativity ($P = 0.032$) and MET status ($P < 0.001$). The *≥70% = 0 or ≥70% = 3+* group was associated with MET status ($P = 0.043$). The *≥70% = 0 or ≥80% = 3+* group showed significant correlations with MSS ($P = 0.029$) and MET status ($P = 0.024$). Finally, the *≥70% = 0 or ≥50% = 3+* and *≥90% = 0 or ≥80% = 3+* groups vs. reminder did not show any correlations with clinicopathological characteristics (data not shown).

The combination of *≥90% = 0 or ≥50% = 3+* correlated with EBV status ($P = 0.007$), miscrosatellite instability ($P = 0.017$), and moreover with the grading ($P = 0.035$) (Table 1). Among the 254 EBV-negative, MSS, and non-diffuse cases, 133 (52.4%) cases fell in the *<90% = 0 or <50% = 3+* group, whereas 121 (47.6%) cases fell in the *≥90% = 0 or ≥50% = 3+* group (Fig. 4).

3.2.4. p53 expression patterns

p53 immunostaining was categorized as *homogeneous* and *heterogeneous* (Fig. 3). The cohort included 414 (88.7%) GCs with a homogeneous and 53 (11.3%) GCs with a heterogeneous staining pattern. The GCs with a homogeneous staining pattern could be further divided into the following three groups: 117 (25.1%) were negative for p53 expression (at least 90% of tumor cells were p53 negative) and were classified as *homogeneous white*, 96 (20.6%) *homogeneous black* cases showed uniform labeling of all tumor cells, and 201 (43.0%) specimens were classified as *homogeneous gray* with positively and negatively stained cells intermixed randomly. A heterogeneous pattern with well-demarcated areas of differently stained tumor cells was present in 10 (2.1%) GCs classified as *black and white*, 21 (4.5%) GCs classified as *black and gray*, and 20 (4.3%) GCs classified as *gray and white* cases. Two specimens showed more than two staining patterns. They were classified as *heterogeneous black-white-gray*. On comparing the *heterogeneous* and *homogeneous* groups, no correlations were found with any clinicopathological characteristic (Table 1).

The correlation of the p53 expression pattern with the second ($P < 0.001$) and third ($P = 0.037$) algorithm of the immunohistochemical evaluation appeared to be significant. The distribution of the 53 *heterogeneous* cases with regard to the different settings of immunohistochemical evaluation showed the following results. Looking at the algorithm dividing the cohort at the median, 31 (58.5%) of the 53 cases were part of the *high* group. Dividing the

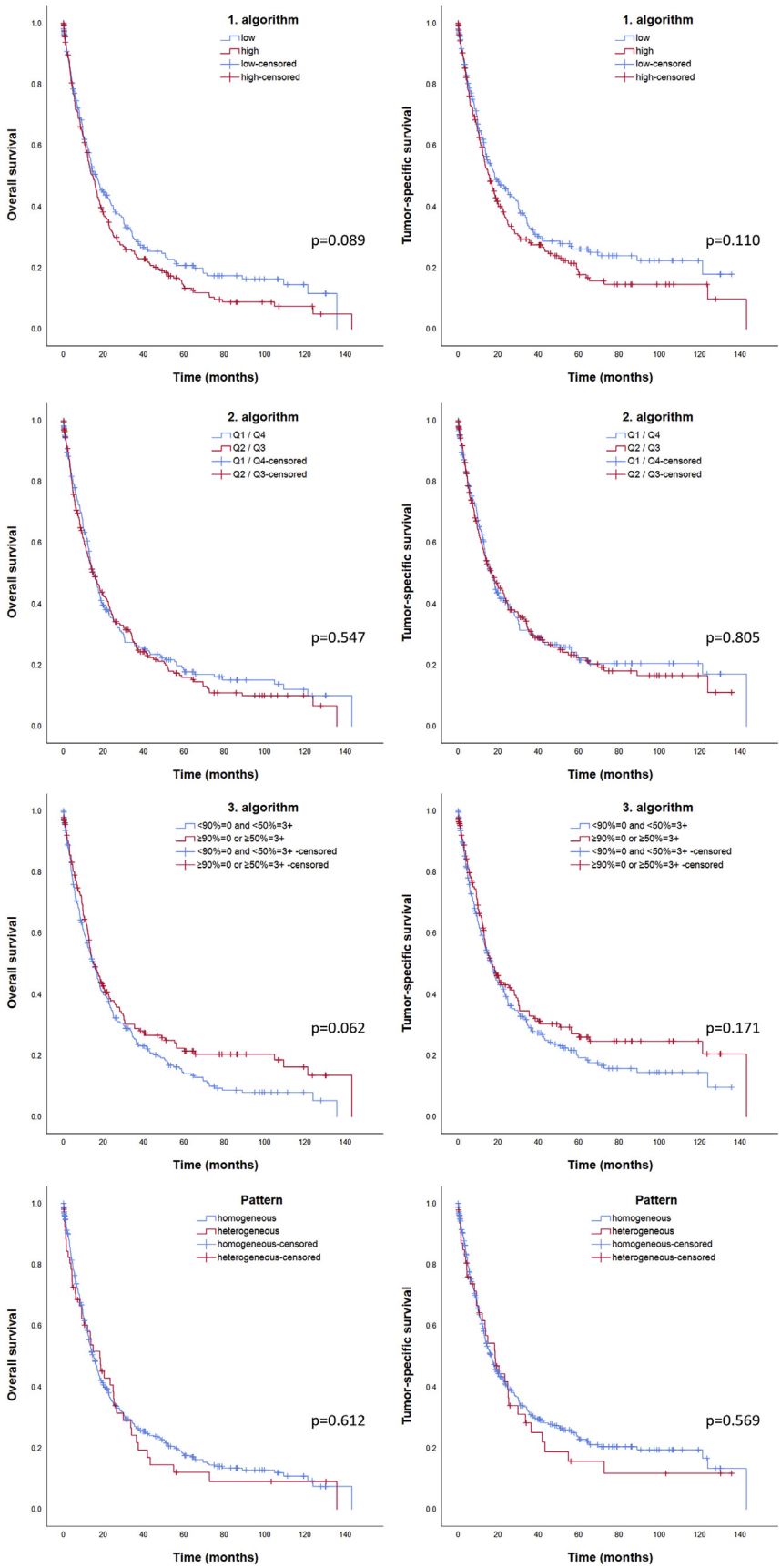

Fig. 5 Overall and tumor-specific survival in different immunostaining evaluation algorithms. The median survival with 95% confidence intervals was determined using the Kaplan-Meier method. Differences between median survivals were tested using the log-rank test.

cohort into quartiles, the outer ones *Q1/Q4* harbored 13 (24.5%) *heterogeneous* cases. The group defined by *≥90% = 0 or 50% = 3+* contained 14 (26.4%) *heterogeneous* GCs. From a different perspective, the *high* group containing 234 GCs harbored 31 (13.2%) *heterogeneous cases*, the *Q1/Q4* group containing 235 GCs harbored 13 (5.5%) *heterogeneous* cases, and the *≥90% = 0 or ≥50% = 3+* group containing 188 GCs harbored 14 (7.4%) *heterogeneous* cases (Table 1).

3.3. TP53 mutational status

To validate the *TP53* mutational status in the *TP53 mutation−related p53 expression−type* GCs in each setting, *TP53* was analyzed via Sanger sequencing. Of all 36 HER2/MET-positive cases (CINe GCs) accessible in this project, genetic analysis turned out successfully in 34 cases. Sixty-nine HER2/MET-negative diffuse-type cases (*GS* GCs) were added to the validation cohort. In addition, of 53 heterogenous cases, two independent DNA extractions of both areas were possible in 23 cases. Here, the gene analyses turned out successfully in 13 cases: 1 CINe, 4 *GS*, and 8 further heterogeneous cases.

p53 immunostaining of the preselected GCs revealed immunonegativity, as well as faint and intense immunostaining in both CINe GCs and *GS* GCs. Sanger sequencing showed that 75 of 111 cases harbored the wild-type TP53 or a silent mutation and 36 cases harbored a mutation other than a silent mutation. Twenty (58.8%) of the 34 cases of HER2/MET-positive intestinal-type GCs harbored TP53 mutations other than the silent mutation, whereas 14 (20.3%) of the 69 HER2/MET-negative diffuse-type cases exhibited a mutation other than the silent one. Regarding the heterogeneous GCs, in 8 cases, the wild-type TP53 was found, 3 cases harbored the same genetic aberration in both heterogeneous areas, and 2 cases showed a mutation only in one of both areas (Fig. 2C and Supplemental Tables 2 and 3).

Comparing the results of all 111 gene analyses and immunostaining, the correlation between mutated TP53 and the *high* HScore was significant ($P < 0.001$). While the *high* group enclosed 26 (72.2%) of the 36 mutated cases, the *Q1/Q4* group harbored 20 (55.6%) mutated cases, and the *≥90% = 0 or ≥50% = 3+* group harbored 17 (47.2%) mutated cases. From a different perspective, the *high* group containing 52 GCs indicated 26 (50.0%) TP53-mutated cases, the *Q1/Q4* group containing 48 GCs indicated 20 (41.7%) TP53-mutated cases, and the *≥90% = 0 or ≥50% = 3+* group containing 42 cases indicated 17 (40.5%) TP53-mutated cases (Table 1).

4. Discussion

The robust classification of a tumor entity into subgroups is one of the basic necessities in surgical pathology. As per TCGA, although the characterization of the subtypes EBV+ and MSI GC is well established and straightforward, differentiation between CIN and GS is less obvious and relies on the analysis of extensive somatic copy number alterations (SCNAs) [3], which is of limited utility in daily practice.

4.1. Indicating the *TP53 mutation−related p53 expression type* by p53 IHC in CINe GC

Chromosomal instability is a genomic instability in which a high rate of mutations appears at the chromosomal level [22]. An important player in chromosomal instability is the TP53 tumor suppressor gene and its protein p53 [3]. Because cancers with frequent gene amplifications, deletions, and aneuploidy are correlated with TP53 mutations [23], one can assume that a cell that is CIN can only escape apoptosis when p53—*the guardian of the genome*—is malfunctional in some way. In our study, we tested the hypothesis that p53 IHC is suitable for predicting TP53 mutation status and thereby CIN GC. We sought an algorithm of p53 IHC, which could be used as a *TP53 mutation−related p53 expression type* [9−12]. In addition, we compared different combinations of immunostaining patterns with typical clinicopathological characteristics of CIN GCs as per TCGA [3].

As per TCGA, 71% of CIN GCs harbor a TP53 mutation [3]. A TP53 mutation might result in the accumulation of the protein in the nucleus [24], but mutations other than missense mutations cannot increase the protein level detected by IHC (reviewed in the study by Fenoglio-Preiser et al. [25]). Ando et al. [9] showed that GCs with strong staining for p53 in 70% of the tumor cell nuclei harbored missense mutations in most cases. Immunonegative cases had a wild-type TP53 in 80% of the cases. The other 20% were mostly nonsense mutated [9]. A loss of protein expression itself can also occur when the whole gene is deleted [25]. Wild-type p53 usually functions in the nucleus, has a short half-life, and, hence, escapes immunodetection. It must be considered that upregulation and detection of p53 are normally caused by physiological circumstances other than mutation. When DNA damage is sensed, the wild-type TP53 is upregulated, and it slows down the cell cycle progression or arrests the cell cycle at G1. This provides time for error correction of the damaged DNA. Upregulated expression of the gene or diminished protein degradation, which is important in its regulation, can lead to nuclear accumulation of the protein. Thus, even very low levels of p53, which do not result from mutations, can sometimes be detected [26]. In summary, under physiological circumstances, p53 IHC would show no or moderate immunostaining. The *TP53 mutation−related p53 expression type* would present itself as a nonimmunostained or strongly immunostained tumor cell nucleus.

In our study, the immunostaining of p53 showed high, low, or no expression in the specimens, in a homogeneous

or heterogeneous pattern. The p53 protein was probably detected in all subgroups, that is, in CIN, GS, EBV+, and MSI GCs. As per TCGA, some GCs considered as CIN do not reveal p53 immunostaining [3]. To evaluate the intensity and pattern of immunostaining systematically, we applied the HScore, which facilitates the evaluation of intensity and percentage of immunostained cells. The multipliers within the formula yield an improved stratification of the IHC. Specifically, tumor samples with a predominantly high staining intensity and those with a predominantly low staining intensity are separated more distinctively. We tried to characterize the *TP53 mutation−related p53 expression type* in different settings of p53 immunohistochemical evaluation as *high* (HScore ≥92), *Q1/Q4* (Q1: HScore ≤15 and Q4: HScore ≥189), and *≥90% (0) or ≥50% (3+)* (more than 90% of nonstained tumor or more than 50% of strongly stained tumor cells). Fig. 2A and B present a graphical representation of the different evaluation algorithms in the entire cohort and also illustrate the continuum of p53 immunostaining in a large GC cohort.

Our results clearly confirmed the significant connection between p53 immunohistochemical and clinicopathological characteristics that are typical for CIN GC. The *Q1/Q4* group appeared to be most suitable to represent CINe GCs. The correlations with the main aspects separating the CIN subtype from the other subtypes of GCs appeared to be significant: EBV negativity ($P < 0.001$), MSS ($P < 0.001$), and an intestinal Laurén phenotype ($P = 0.041$). The distribution of only EBV-negative, MSS, and intestinal GCs into the groups of this algorithm showed that 161 (63.4%) cases belonged to the *Q1/Q4* group and 93 (36.6%) cases belonged to the *Q2/Q3* group, reproducing TCGA's observation of 71% TP53-mutated CIN GCs most exactly (Fig. 4).

It was impossible to select one most meaningful third algorithm of the different approaches related to the raw percentages of p53 IHC. Different sets of percentages showed correlations with different clinicopathological characteristics, but no approach stood out obviously (data not shown). As correlating with both EBV negativity ($P=0.007$) and MSS ($P=0.017$), the algorithm *≥90% = 0 or ≥50% = 3+* versus *<90% = 0 and <50% = 3+* (setting the limits more generously than *≥99% = 0 or ≥50% = 3* versus *<99%=0 and <50%=3*) was chosen as a representative for further examination. Overall, this approach did not lead to more meaningful findings, and it did not seem to have an advantage over *Q1/Q4* versus *Q2/Q3* in CIN GC diagnostics.

TP53 was sequenced to validate the results we had obtained by IHC and to determine whether GCs identified as *TP53 mutation−related p53 expression−type* GCs by immunohistochemical evaluation might harbor TP53 mutations. To understand the functional status of p53 detected in both CIN and GS GC, the TP53 gene was screened for mutations in a validation cohort of 111 GCs that were selected based on previously obtained molecular characteristics and that consisted of EBV and MSS subtypes [17,18,19,20] or had an easily separable heterogeneous staining pattern. This validation cohort contained 34 likely CIN and 69 likely GS GCs, as characterized by their respective HER2/MET status and Laurén phenotype. Specifically, HER2-positive and/or MET-positive intestinal-type GCs were characterized as CINe, and HER2-negative and MET-negative diffuse-type GCs were characterized as GS as per TCGA [3]. The p53 HScores in all positive cases showed an overall lower range in HER2/MET-negative GCs than in HER2/MET-positive cancers. As anticipated, most rather strongly p53-stained CINe GCs had a missense mutation. Regarding little p53-stained or p53-negative CINe GCs, four cases harbored frameshift mutations.

Interestingly, we could not validate the CINe GCs indicated by *Q1/Q4* that equaled the *TP53 mutation−related p53 expression−type* to in fact represent TP53 mutations. Instead, the first algorithm *high* vs. *low* showed a significant relationship with the TP53 mutational status ($P < 0.001$). The definition of CIN implies a high level of mutagenic potential at the chromosomal level. In a biallelic cell, a heterozygous TP53 mutation would lead to one functional and 15 dysfunctional or nonfunctional p53 versions because the protein's structure as a tetramer causes a dominant negative effect. This means that, in CIN tumor cells, polyploid genetic material harbors more than a biallelic base of TP53, leading to more than 16 possible combinations of the tetramer. In addition, the regulation of TP53 is complex. It has alternative splice and translation sites. The protein has up to 10 isoforms, and it is activated by post-translational modifications [27]. In addition, epigenetic modifications [28] and microRNAs regulate its expression, making the detection of an active protein difficult [29]. Many different mutations of the TP53 itself, or of the p53 pathway or metabolism-regulating genes, may come together in one cell rather leading to a *gray scale* of p53 expression not resulting in a negative (nonsense mutation of TP53) or strongly positive (missense mutation of TP53) p53 IHC. Moreover, p53 monomers and dimers can fulfill a subfunction; for example, dimeric p53 variants are cytostatic, and they can arrest cell growth [30], further extending the *gray scale* of function of p53 variants. In physiological circumstances, because chromosomal instability would normally end up exhibiting apoptosis among other factors owing to p53 function, CIN GC cells appear to be connected with the outer extremes of this *gray scale* (*Q1/Q4*). As a result, p53 IHC might still offer a convincing approach toward capturing CIN GCs affected by a malfunction of p53 regulation. Meanwhile, TP53 mutations appear to rather correlate with a *high* HScore, which might result from the fact that TP53 mutations are more common in strongly stained than in nonstained cells [9]. p53 malfunctional cases and TP53-mutated cases appear not to be congruent.

In the end, we could not validate our initial hypothesis of defining a *TP53 mutation−related p53 expression−type*

tumor via the use of p53 IHC, while the connection between p53 immunohistochemical and clinicopathological characteristics typically found in CINe GCs was left standing. Our results relate to a large cohort, but individual cases did not demonstrate the applicability of the concept.

4.2. Heterogeneity of p53 expression detected by IHC in CINe GC

We paid special attention to the intratumoral heterogeneity of p53 protein expression in GC. Chromosomal instability may be considered as a driver of tumor heterogeneity in diverse cancers, including GC. It generates cellular and, hence, subclonal diversity at the genetic level of solid tumors. During tumor progression, these subclones undergo selection and form the basis of tumor evolution and intratumor diversity [31]. Böger et al. [17] have recently shown that a single primary GC can harbor up to five different PIK3CA genotypes. Similarly, HER2- and MET-amplified and HER2- and MET-unamplified tumor cell clones were found within the same primary GC [19,20,32]. As chromosomal instability promotes tumor evolution and stimulates microenvironmental selection of cancer cell clones, identifying chromosomal instability as such in GC tissue samples and biopsies might be important. Chemotherapy may be viewed as another microenvironmental cue for tumor evolution, making CIN tumors particularly *fit for survival*.

Our study confirmed the existence of intratumoral heterogeneity of p53 expression by IHC. To evaluate whether heterogeneous cases might harbor discordant mutations, such as missense and nonsense mutations, in the same primary tumor [9], we reexamined the TP53 mutational status in 13 GCs with a distinct pattern of immunostaining. Positive and negative sections were sequenced individually to ensure no cross contamination of the regions and to assess the heterogeneity of TP53 mutational status. The analyses showed wild-type TP53 in 8 cases and mutated TP53 in 3 cases harboring the same mutation in both areas. In two cases (case no. 102 and 104), the presence of possible different TP53 mutations in one GC with different manifestations of p53 protein expression could be confirmed (Fig. 2C, Supplemental Tables 2 and 3). The p53 immunohistochemical pattern showed no significant correlation with TP53 mutational status.

p53 malfunctions are a driver for genomic instability, for example, chromosomal instability, which possibly occurs early during tumor evolution, leading to an intratumoral heterogeneity [33]. Conversely, the resulting subclonal genetic diversity of CIN GC may affect subclonal p53 pathway regulation, leading to an intratumoral heterogeneity of the p53 expression pattern. Thus, a heterogeneous pattern of p53 expression rather reflects overall subclonal diversity of CIN GC than intratumoral heterogeneity of TP53 mutational status.

4.3. Conclusion

The existence of an intratumoral heterogeneity of p53 expression in GC could be confirmed. Thus, biopsies do not seem to be suitable for assessing p53 positivity in GC. This study aimed to find an algorithm for evaluating p53 expression in IHC to predict enrichment of chromosomal instability in GC. In the whole cohort, our results clearly show that the IHC of p53, TP53 mutational status, and the CIN subtype were connected. However, different algorithms for p53 immunohistochemical evaluation cannot be used to predict TP53 mutations and, hence, chromosomal instability in individual cases. The p53 expression in GC is neither related to the overall nor related to the TSS in GC and has no prognostic utility in diagnostic pathology of GC.

Compliance with ethical standards

This study was performed as per the Declaration of Helsinki. Ethical approval was obtained from the local ethical review board (D 453/10). After study inclusion, data from all patients were pseudonymized.

Appendix A. Supplementary data

Supplementary data to this article can be found online at https://doi.org/10.1016/j.humpath.2020.09.006.

Acknowledgments

Study concept and design was contributed by I.S., S.S.M., and C.R. Surgical pathological data were acquired by I.S., S.S.M., and C.R. Molecular pathological analysis were conducted by I.S., S.S.M., S.K., and J.H. The data were analyzed and interpreted by I.S., S.S.M., J.H., H.-M.B., and C.R. Drafting of the manuscript and critical revision of the manuscript for important intellectual content was carried out by all the authors. Administrative, technical, or material support was provided by S.K., J.H., and C.R. The study was supervised by C.R.

References

[1] Robert-Koch-Institut. Krebs in Deutschland für 2013/2014: gemeinsame Publikation des Zentrums für Krebsregisterdaten und der Gesellschaft der epidemiologischen Krebsregister in Deutschland e.V., 32-35.

[2] Correa P. Human gastric carcinogenesis: a multistep and multifactorial process–first American cancer society award Lecture on cancer Epidemiology and prevention. Cancer Res 1992;52:6735−40.

[3] Cancer Genome Atlas Research N. Comprehensive molecular characterization of gastric adenocarcinoma. Nature 2014;513:202−9. https://10.1038/nature13480.

[4] Lei Z, Tan IB, Das K, Deng N, Zouridis H, Pattison S, et al. Identification of molecular subtypes of gastric cancer with different responses to PI3-kinase inhibitors and 5-fluorouracil. Gastroenterology 2013;145:554−65. https://10.1053/j.gastro.2013.05.010.

[5] Setia N, Agoston AT, Han HS, Mullen JT, Duda DG, Clark JW, et al. A protein and mRNA expression-based classification of gastric cancer. Mod Pathol 2016;29:772–84. https://10.1038/modpathol.2016.55.
[6] Tannock IF, Hickman JA. Limits to personalized cancer medicine. N Engl J Med 2016;375:1289–94. https://10.1056/NEJMsb1607705.
[7] Cristescu R, Lee J, Nebozhyn M, Kim KM, Ting JC, Wong SS, et al. Molecular analysis of gastric cancer identifies subtypes associated with distinct clinical outcomes. Nat Med 2015;21:449–56. https://10.1038/nm.3850.
[8] Gonzalez RS, Messing S, Tu X, McMahon LA, Whitney-Miller CL. Immunohistochemistry as a surrogate for molecular subtyping of gastric adenocarcinoma. Hum Pathol 2016;56:16–21. https://10.1016/j.humpath.2016.06.003.
[9] Ando K, Oki E, Saeki H, Yan Z, Tsuda Y, Hidaka G, et al. Discrimination of p53 immunohistochemistry-positive tumors by its staining pattern in gastric cancer. Cancer Med 2015;4:75–83. https://10.1002/cam4.346.
[10] Xue Y, San Luis B, Lane DP. Intratumour heterogeneity of p53 expression; causes and consequences. J Pathol 2019;249:274–85. https://10.1002/path.5328.
[11] Itaya M, Yoshimoto J, Kojima K, Futagawa S. Usefulness of p53 protein, Bcl-2 protein and Ki-67 as predictors of chemosensitivity of malignant tumors. Oncol Rep 1999;6:675–82. https://10.3892/or.6.3.675.
[12] Köbel M, Piskorz AM, Lee S, Lui S, LePage C, Marass F, et al. Optimized p53 immunohistochemistry is an accurate predictor of TP53 mutation in ovarian carcinoma. J Pathol Clin Res 2016;2:247–58. https://10.1002/cjp2.53.
[13] Cancer Genome Atlas Research N. Analysis Working Group: asan U, Agency BCC, et al. Integrated genomic characterization of oesophageal carcinoma. Nature 2017;541:169–75. https://10.1038/nature20805.
[14] Brierley J, Gospodarowicz MK, Wittekind C. TNM classification of malignant tumours. Wiley Blackwell; 2016.
[15] Lauren P. The two histologic main types of gastric carcinoma: Diffuse and so-called intestinal-type carcinoma. Acta Pathol Microbiol Scand 1965;64:31–49.
[16] Warneke V, Behrens HM, Haag J, Balschun K, Böger C, Becker T, et al. Prognostic and putative predictive biomarkers of gastric cancer for personalized medicine. Diagn Mol Pathol 2013;22:127–37. https://10.1097/PDM.0b013e318284188e.
[17] Böger C, Krüger S, Behrens HM, Bock S, Haag J, Kalthoff H, et al. Epstein-Barr virus-associated gastric cancer reveals intratumoral heterogeneity of PIK3CA mutations. Ann Oncol 2017;28:1005–14. https://10.1093/annonc/mdx047.
[18] Mathiak M, Warneke VS, Behrens HM, Haag J, Böger C, Krüger S, et al. Clinicopathologic characteristics of microsatellite instable gastric carcinomas revisited: urgent need for standardization. Appl Immunohistochem Mol Morphol 2017;25:12–24. https://10.1097/PAI.0000000000000264.
[19] Warneke VS, Behrens HM, Böger C, Becker T, Lordick F, Ebert MP, et al. Her2/neu testing in gastric cancer: evaluating the risk of sampling errors. Ann Oncol 2013;24:725–33. https://doi.org/10.1093/annonc/mds528. https://mds528 [pii].
[20] Metzger ML, Behrens HM, Böger C, Haag J, Krüger S, Röcken C. MET in gastric cancer - discarding a 10% cutoff rule. Histopathology 2016;68:241–53. https://10.1111/his.12745.
[21] Simes RJ. An improved Bonferroni procedure for multiple tests if signficance. Biometrika 1986;73:751–4.
[22] Maleki SS, Röcken C. Chromosomal Instability in gastric cancer biology. Neoplasia 2017;19:412–20. https://10.1016/j.neo.2017.02.012.
[23] Overholtzer M, Rao PH, Favis R, Lu XY, Elowitz MB, Barany F, et al. The presence of p53 mutations in human osteosarcomas correlates with high levels of genomic instability. Proc Natl Acad Sci U S A 2003;100:11547–52. https://10.1073/pnas.1934852100.
[24] Giaccia AJ, Kastan MB. The complexity of p53 modulation: emerging patterns from divergent signals. Genes Dev 1998;12:2973–83. https://10.1101/gad.12.19.2973.
[25] Fenoglio-Preiser CM, Wang J, Stemmermann GN, Noffsinger A. TP53 and gastric carcinoma: a review. Hum Mutat 2003;21:258–70. https://10.1002/humu.10180.
[26] Ashcroft M, Vousden KH. Regulation of p53 stability. Oncogene 1999;18:7637–43. https://10.1038/sj.onc.1203012.
[27] Hollstein M, Hainaut P. Massively regulated genes: the example of TP53. J Pathol 2010;220:164–73. https://10.1002/path.2637.
[28] Murao K, Kubo Y, Ohtani N, Hara E, Arase S. Epigenetic abnormalities in cutaneous squamous cell carcinomas: frequent inactivation of the RB1/p16 and p53 pathways. Br J Dermatol 2006;155:999–1005. https://10.1111/j.1365-2133.2006.07487.x.
[29] Kumar M, Lu Z, Takwi AA, Chen W, Callander NS, Ramos KS, et al. Negative regulation of the tumor suppressor p53 gene by microRNAs. Oncogene 2011;30:843–53. https://10.1038/onc.2010.457.
[30] Fischer NW, Prodeus A, Malkin D, Gariepy J. p53 oligomerization status modulates cell fate decisions between growth, arrest and apoptosis. Cell Cycle 2016;15:3210–9. https://10.1080/15384101.2016.1241917.
[31] Bakhoum SF, Landau DA. Chromosomal Instability as a Driver of tumor Heterogeneity and evolution. Cold Spring Harb Perspect Med 2017;7. https://10.1101/cshperspect.a029611.
[32] Iwamatsu H, Nishikura K, Watanabe H, Ajioka Y, Hashidate H, Kashimura H, et al. Heterogeneity of p53 mutational status in the superficial spreading type of early gastric carcinoma. Gastric Cancer 2001;4:20–6. https://10.1007/s101200100012.
[33] Kastenhuber ER, Lowe SW. Putting p53 in context. Cell 2017;170:1062–78. https://10.1016/j.cell.2017.08.028.